Topology optimization of single and double panels for improved sound insulation in specific frequency bands

Daniele Giannini[1]
Department of Civil Engineering - Structural Mechanics Section, KU Leuven
Kasteelpark Arenberg 40, 3001 Leuven, Belgium

Mattias Schevenels[2]
Department of Architecture - Architectural Engineering Research Group, KU Leuven
Kasteelpark Arenberg 1, 3001 Leuven, Belgium

Edwin Reynders[3]
Department of Civil Engineering - Structural Mechanics Section, KU Leuven
Kasteelpark Arenberg 40, 3001 Leuven, Belgium

ABSTRACT

In this work, we investigate the potential of considering a non-uniform material distribution in the design of panel partitions, in order to achieve a superior vibroacoustic performance close to a given target frequency. In order to achieve this goal, we apply numerical topology optimization to find the optimal material thickness distribution for both single and double panels. Two formulations of the optimization problem are employed: in the first one, we suppress the resonance dips in the sound transmission loss by simply pushing the system eigenfrequencies far away from the target frequency. In the second formulation, we directly maximize the sound transmission loss of the system at the target frequency. In the iterative design process, the panels are modelled by mechanical plate finite elements. For double panels, the vibro-acoustic coupling between the panels and the internal air cavity, which is modelled analytically, is accounted for. The sound insulation properties are evaluated by transmission loss computations through hybrid Deterministic-Statistical Energy Analysis (Det-SEA) simulations. The method is applied considering different target frequencies in the audible range and focusing on practically relevant design cases. For both single PMMA panels and double glazing panels, it is demonstrated how a non-uniform thickness distribution allows for significant transmission loss improvements close to the target frequency, that are in the range of 5-15 dB with respect to uniform panels with the same mass.

[1]daniele.giannini@kuleuven.be

[2]mattias.schevenels@kuleuven.be

[3]edwin.reynders@kuleuven.be

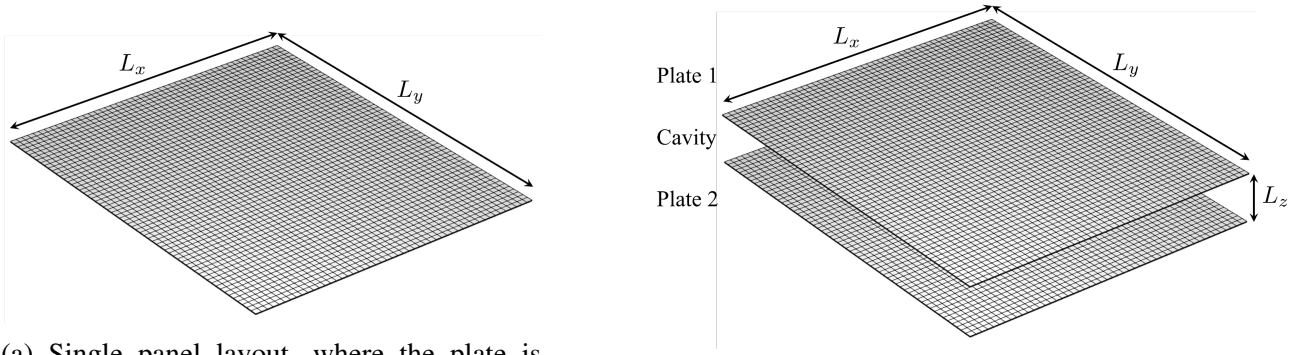

(a) Single panel layout, where the plate is discretized by finite elements.

(b) Double panel layout, where the two plates are discretized by finite elements.

Figure 1: Layout of single and double panels.

1. INTRODUCTION

Single and double panels are commonly employed in noise control, e.g., as partitioning elements between rooms and to enclose noisy machines. When focusing on specific frequency ranges, e.g. in presence of narrowband disturbances related for example to rotating machines, further improvements in sound insulation can be obtained by non-uniformly distributing the material within the area of the panels, i.e. considering a varying thickness within the panel area. The suitability of this design approach has been demonstrated for single panels, for which topology optimization [1] has been employed to achieve an efficient design procedure.

In [2], the thickness distribution within the panel area has been optimized to achieve a maximum sound Transmission Loss (TL) in specific frequency bands, while employing a hybrid deterministic - statistical energy analysis (Det-SEA) model [3], in which the deterministic (FE) model of the plate is coupled with the sound fields in the source and receiving rooms, modelled as diffuse (SEA) subsystems. Following different works in topology optimization that focus on eigenfrequencies control to obtain the desired dynamic vibroacoustic performance [4–6], in [7] the thickness distribution in single panels has been optimized to push the structural eigenfrequencies as far as possible from a given disturbance frequency. The optimal layouts were found relying on an in-vacuo mechanical finite element model of a simply supported plate, that allows for a computationally efficient optimization. The sound insulation performance of the optimized layouts were verified a posteriori through Det-SEA simulations, showing the effectiveness of the chosen design strategy in avoiding resonance dips in the TL curve.

In this paper, the two different design strategies presented in [2] and [7] are compared for a selected design case of PMMA single panels, and then extended towards double glazing panels, when considering in the deterministic model of the panel the vibroacoustic coupling between the mechanical plates and the acoustic cavity.

The paper is organized as follows. Section 2 describes the vibroacoustic modelling employed for single and double panels. Section 3 introduces the design variables of the topology optimization problem, along with the two proposed formulations of objective and constraints, and the considered solution procedure. The optimized layouts and their vibroacoustic performance are discussed in Section 4, while Section 5 gives some conclusions and remarks.

2. VIBROACOUSTIC MODELLING OF THE PANEL

Referring to Figure 1, the focus of the present work will be both on single panels and on double panels, consisting of two single panels separated by an air cavity. In this Section, the modeling strategy for the different panel components, and their coupling, will be described: the focus will be

on the more general case of a double panel with 3 components (plate-cavity-plate), while the single panel can be treated as a related simplification when only one plate is considered.

2.1. Model of the panel components

Following what proposed in [8], the out-of-plane displacement fields of the two plates, $u_1(\boldsymbol{x}, \omega)$ and $u_2(\boldsymbol{x}, \omega)$, and the pressure field within cavity, $p_{cav}(\boldsymbol{x}, \omega)$, at spatial location $\boldsymbol{x}$ and frequency ω, are approximate using a set of basis functions $\boldsymbol{\Phi}$ that correspond to generalized coordinates $\boldsymbol{q}$:

$$\begin{aligned} u_1(\boldsymbol{x}, \omega) &= \boldsymbol{\Phi}_1(\boldsymbol{x})\boldsymbol{q}_1(\omega) \\ u_2(\boldsymbol{x}, \omega) &= \boldsymbol{\Phi}_2(\boldsymbol{x})\boldsymbol{q}_2(\omega) \\ p_{cav}(\boldsymbol{x}, \omega) &= \boldsymbol{\Phi}_{cav}(\boldsymbol{x})\boldsymbol{q}_{cav}(\omega) \end{aligned} \tag{1}$$

The basis functions in $\boldsymbol{\Phi}_p = \left[\boldsymbol{\phi_{p,1}}, ..., \boldsymbol{\phi_{p,n_p}}\right]$ $(p = 1, 2)$, used to describe the displacement fields in the plate, are the mass-normalized mode shapes of the in-vacuo mechanical plate. The eigenfrequencies $\omega_{p,k}$ and the modal shapes $\boldsymbol{\phi}_{p,k}$ of the p-th plate can be found by solving the following eigenvalue problem:

$$(\omega_{p,k}^2 \boldsymbol{M_p} + \boldsymbol{K_p})\boldsymbol{\phi_{p,k}} = \boldsymbol{0} \tag{2}$$

where $\boldsymbol{M_p}$ and $\boldsymbol{K_p}$ are the mass and stiffness matrices of the plate, coming from finite element discretization (cf. Figure 1), and the eigenfrequencies in Hz can be found as $f_{p,k} = \omega_{p,k}/2\pi$. p is the index of the plate, i.e. $p = 1$ for single panels and $p = 1, 2$ for double panels. In particular, for both single and double panels each plate is discretized by Kirchhoff plate elements and modelled as simply supported on its four edges.

The basis functions $\boldsymbol{\Phi}_{cav} = [\boldsymbol{\phi_{cav,1}}, ..., \boldsymbol{\phi_{cav,n_{cav}}}]$ are instead chosen as the analytically computed normalized mode shapes of the decoupled, hard-walled, rectangular cuboid cavity:

$$\phi_{cav,k}(\boldsymbol{x}) = a_k \cos\left(\frac{m_k \pi x}{L_x}\right) \cos\left(\frac{n_k \pi y}{L_y}\right) \cos\left(\frac{p_k \pi z}{L_z}\right) \tag{3}$$

where L_x,L_y are the in-plane dimensions of the plates and the cavity, L_z is the cavity depth (cf. Figure 1), $m_k \in \mathbb{N}_0$, $n_k \in \mathbb{N}_0$ and $p_k \in \mathbb{N}_0$ are the number of half wavelengths in the x, y and z coordinate directions. The normalization constant satisfies

$$a_k = \frac{c_a \gamma(m_k)\gamma(n_k)\gamma(p_k)}{\sqrt{L_x L_y L_z}} \qquad \text{with:} \qquad \gamma(s) = \begin{cases} \sqrt{2} & \text{if } s \neq 0 \\ 1 & \text{if } s = 0 \end{cases} \tag{4}$$

and $c_a = 343$ m/s is the speed of sound in air. The angular natural frequency correspoding to mode k equals:

$$\omega_{cav,k} = c_a \sqrt{\left(\frac{m_k \pi y}{L_x}\right)^2 + \left(\frac{n_k \pi}{L_y}\right)^2 + \left(\frac{p_k \pi}{L_z}\right)^2} \tag{5}$$

2.2. Fluid-structure interaction at the cavity boundaries

Let's now consider the coupling between the cavity and the panel plates. The load onto the k-th mode of the first plate, due to the cavity pressure $p_{cav}(\boldsymbol{x}, \omega)$, can be expressed as [8]:

$$\begin{aligned} f_{1,k,cav}(\omega) &= -\int_{\Gamma_1} \phi_{1,k}(\boldsymbol{x}) p_{cav}(\boldsymbol{x}, \omega) d\boldsymbol{x} \approx -\sum_{l=1}^{n_{cav}} L_{f1,kl} q_{cav,l}(\omega) \\ \text{where: } L_{f1,kl} &= \int_{\Gamma_1} \phi_{1,k}(\boldsymbol{x}) \phi_{cav,l}(\boldsymbol{x}) d\boldsymbol{x} \end{aligned} \tag{6}$$

where Γ_1 denotes the interface surface area between the plate and the cavity.

The load onto the k-th mode of the cavity, due to the displacement of the first plate $u_1(\boldsymbol{x}, \omega)$, can be expressed as [8]:

$$f_{cav,k,1} = -\rho_a \omega^2 \int_{\Gamma_1} \phi_{cav,k}(\boldsymbol{x}) u_1(\boldsymbol{x}, \omega) \approx -\sum_{l=1}^{n_1} L_{s1,kl} q_{1,l}(\omega)$$
$$\text{where } L_{s1,kl} := \rho_a \omega^2 L_{f1,kl} \tag{7}$$

where $\rho_a = 1.20$ kg/m^3 is density of air. The number of considered modes n_p ($p = 1,2$) and n_{cav}, for the plates and the cavity respectively, is such that we retain all the modes below 2 times the frequency of the analysis.

2.3. Model of the coupled system

The equations of motion of the coupled panel system, in terms of the generalized coordinates of its components, will be:

$$\begin{bmatrix} \boldsymbol{D}_1 & \boldsymbol{0} & \boldsymbol{L}_{f1} \\ \boldsymbol{0} & \boldsymbol{D}_2 & \boldsymbol{L}_{f2} \\ \boldsymbol{L}_{s1} & \boldsymbol{L}_{s2} & \boldsymbol{D}_{cav} \end{bmatrix} \begin{Bmatrix} \boldsymbol{q}_1 \\ \boldsymbol{q}_2 \\ \boldsymbol{q}_{cav} \end{Bmatrix} = \begin{Bmatrix} \boldsymbol{f}_1 \\ \boldsymbol{f}_2 \\ \boldsymbol{0} \end{Bmatrix} \qquad \Rightarrow \qquad \boldsymbol{D}_d \boldsymbol{q} = \boldsymbol{f} \tag{8}$$

Where $\boldsymbol{D}_1$, $\boldsymbol{D}_2$, $\boldsymbol{D}_{cav}$ represent the dynamic stiffness matrices of the plates and the cavity, that refer to the generalized coordinates related to the normalized modes. The $\boldsymbol{f}$ vectors represent instead external fluid loading onto the plates, e.g. due to the acoustic pressure in the adjoining rooms.

In particular, the dynamic stiffness matrix of the p-th plate $\boldsymbol{D}_p$ is a diagonal matrix with entries:

$$D_{1,kk} = -\omega^2 + \omega_{1,k}^2 (1 + i\eta_{1,k}), \tag{9}$$

where $i := \sqrt{-1}$ is the imaginary unit and $\eta_{1,k}$ denotes the damping loss factor of mode k.

The dynamic stiffness matrix $\boldsymbol{D}_{cav}$ of the cavity is instead a diagonal matrix with entries:

$$D_{cav,kk} = -\omega^2 + \omega_{cav,k}^2 (1 + i\eta_{cav,k} k) \tag{10}$$

and $\eta_{cav,k}$ denotes the damping loss factor of mode k. We here consider an empty cavity and determine the modal loss factor from $\eta_{cav,k} = \frac{4.4\pi}{\omega_{cav,k} T_{cav}}$, for a chosen reverberation time $T_{cav} = 2$ s.

When considering homogenous equations of motions, the eigenfrequencies ω_k and the modal shapes $\boldsymbol{\phi_k}$ of the coupled system can be found by solving the following eigenvalue problem:

$$\left(\begin{bmatrix} \boldsymbol{K}_{m,1} & \boldsymbol{0} & \boldsymbol{L}_{f1} \\ \boldsymbol{0} & \boldsymbol{K}_{m,2} & \boldsymbol{L}_{f2} \\ \boldsymbol{0} & \boldsymbol{0} & \boldsymbol{K}_{m,cav} \end{bmatrix} - \omega_k^2 \begin{bmatrix} \boldsymbol{M}_{m,1} & \boldsymbol{0} & \boldsymbol{0} \\ \boldsymbol{0} & \boldsymbol{M}_{m,2} & \boldsymbol{0} \\ -\rho_a \boldsymbol{L}_{f1} & -\rho_a \boldsymbol{L}_{f2} & \boldsymbol{M}_{m,cav} \end{bmatrix} \right) \boldsymbol{\phi_k} = \boldsymbol{0} \tag{11}$$

where $\boldsymbol{M}_{m,p}$, $\boldsymbol{K}_{m,p}$ ($p = 1, 2$) are the modal mass and stiffness matrices of the plates, while $\boldsymbol{M}_{m,cav}$, $\boldsymbol{K}_{m,cav}$ are the modal mass and stiffness matrices of the cavity.

2.4. Transmission suite

In what follows, the model of the panel will be coupled to the sound fields in the adjoining rooms, in order to compute the sound transmission loss (TL) of the panel through the hybrid Deterministic-Statistical Energy Analysis (Det-SEA) modelling framework [3, 9]. While the panel is modelled deterministically to capture its vibroacoustic behaviour in full detail, the sound fields in the source and receiver rooms are modelled as random diffuse (SEA) subsystems. The diffuse sound fields in the transmission rooms and the deterministic plate model are coupled by employing the

diffuse field reciprocity relationship [10], resulting in a full transmission suite (room-panel-room) model [3, 11, 12]. This Det-SEA model yields the diffuse field transmission loss of the (single or double) panel, accounting for its finite size and boundary conditions.

The sound transmission loss is computed as $TL = 10\log(1/\tau)$, where the sound transmission coefficient τ is defined as the ratio between the power flow from the source room (room 1) to the receiver room (room 2) through the panel and the incident sound power on the panel in the source room. τ can be computed from the so-called coupling loss factor η_{12} between the rooms as:

$$\tau = \frac{4V_1\omega}{L_x L_y c}\eta_{12} \tag{12}$$

where V_1 denotes the volume of the sending room.

Within the hybrid Det-SEA framework, the coupling loss factor η_{12} can be evaluated by considering the interaction between the panel and the direct field response of the rooms, i.e. the sound field that would occur if the rooms would behave as acoustic half-spaces. The related so-called direct field dynamic stiffness matrix of the room describes the relationship between the (generalized) displacements of the plate $\boldsymbol{q}_p$ and the interface forces $\tilde{\boldsymbol{f}}_{dir,p}$ due to the pressure field in the acoustic half-space. For example, for room 1:

$$\boldsymbol{D}_{dir1}\boldsymbol{q}_1 = \tilde{\boldsymbol{f}}_{dir1} \tag{13}$$

The direct field dynamic stiffness matrix $\boldsymbol{D}_{dir1}$ can be numerically computed via evaluation of the Rayleigh integral, e.g. using a wavelet discretization of the baffled interface [13].

After computing the direct field acoustic dynamic stiffness matrices of both rooms, the coupling loss factor is obtained from

$$\eta_{12} = \frac{2}{\pi\omega n_1}\sum_{rs}\Im(\boldsymbol{D}'_{dir2,rs})(\boldsymbol{D}_{tot}^{-1}\Im(\boldsymbol{D}'_{dir1})\boldsymbol{D}_{tot}^{-H})_{rs} \tag{14}$$

where $\boldsymbol{D}_{tot}$ is the total dynamic stiffness matrix of the system, and $\boldsymbol{D}'_{dir1}$ and $\boldsymbol{D}'_{dir2}$ are the direct field acoustic dynamic stiffness matrices expressed in terms of the reduced panel coordinate vector:

$$\boldsymbol{D}_{tot} := \boldsymbol{D}_d + \boldsymbol{D}'_{dir1} + \boldsymbol{D}'_{dir2}, \qquad \boldsymbol{D}'_{dir1} = \begin{bmatrix} \boldsymbol{D}_{dir1} & 0 & 0 \\ 0 & 0 & 0 \\ 0 & 0 & 0 \end{bmatrix}, \qquad \boldsymbol{D}'_{dir2} = \begin{bmatrix} 0 & 0 & 0 \\ 0 & \boldsymbol{D}_{dir2} & 0 \\ 0 & 0 & 0 \end{bmatrix} \tag{15}$$

3. TOPOLOGY OPTIMIZATION PROBLEM

3.1. Design variables

Once the modelling framework has been established for the computation of both system eigenfrequencies and sound transmission loss, a set of design variables is chosen in order to describe the material thickness distribution to be optimized.

The thickness distribution within each plate area is described by considering a design variable $\gamma_e \in [0, 1]$ for each e-th finite element. The set of design variables $\boldsymbol{\gamma}$ is used to scale the thickness of the elements, but first a convolution filter is applied [14], in order to avoid mesh dependence of the solution and convergence to checkerboard layouts. The filtered design variables are obtained as:

$$\tilde{\gamma}_e = \frac{\sum_{j\in\mathbb{N}_{s,e}} w(\boldsymbol{x_j})A_j\gamma_{e,j}}{\sum_{j\in\mathbb{N}_{s,e}} w(\boldsymbol{x_j})A_j} \tag{16}$$

where A_j is the area of the j-th element and $\mathbb{N}_{s,e}$ is the set of elements lying within a circle with radius r_{min} centred on the centroid of element e, and belonging to the same plate. The linear weighting function $w(\boldsymbol{x_j})$ is given as:

$$w(\boldsymbol{x_j}) = r_{min} - |\,\boldsymbol{x_j} - \boldsymbol{x_e}\,| \tag{17}$$

where $\boldsymbol{x_j} = (x_j, y_j)$ and $\boldsymbol{x_e} = (x_e, y_e)$ are the centroid coordinates of elements j and e.
The filtered design variables are used to scale the element thicknesses between a minimum value t_{min} and a maximum value t_{max}, and then to accordingly scale the element stiffness and mass matrices [7]:

$$t_e = t_{min} + (t_{max} - t_{min}) \cdot \tilde{\gamma}_e \qquad \Rightarrow \qquad \boldsymbol{K_e}(t_e) = \boldsymbol{K_e}(t = 1) \cdot t_e^3, \qquad \boldsymbol{M_e}(t_e) = \boldsymbol{M_e}(t = 1) \cdot t_e \quad (18)$$

The scaled element matrices are finally assembled to find the global plate stiffness and mass matrices $\boldsymbol{K_p}$ and $\boldsymbol{M_p}$ used in Equation 2.

3.2. Problem formulations

Following [2] and [7], two formulations of the topology optimization problem are used.

In the first formulation (F1), the objective is to find the optimal thickness distribution that maximizes the width of the frequency band without any structural eigenfrequencies around a given target frequency f_c. This is achieved by considering the following objective function and constraints:

$$\begin{aligned} \max_{\gamma} \quad & \beta = \min_i \left(\frac{|f_i - f_c|}{f_c} \right) \\ \text{subject to} \quad & t_{avg,p} = \frac{\sum_{e_p} t_{e_p} A_{e_p}}{\sum_{e_p} A_{e_p}} \leq \frac{t_{min} + t_{max}}{2} \qquad \forall p \end{aligned} \quad (19)$$

We therefore formulate a max-min problem, in which we maximize the minimum normalized distance $\frac{|f_i - f_c|}{f_c}$ between the eigenfrequencies f_i and the target frequency f_c. An additional constraint is imposed to set the maximum material usage, by prescribing that for each plate the average thickness $t_{avg,p}$ should not exceed the mean value between t_{min} and t_{max}. The computation of the eigenfrequencies follows Equation 2 for single plates, where the simple finite element model of the in-vacuo mechanical plate is considered. For double plates, we instead compute the eigenfrequencies through Equation 11, when considering the coupled plate-cavity-plate system.

In the second formulation (F2), we instead maximize the sound transmission loss (TL) computed at the target frequency f_c:

$$\begin{aligned} \max_{\gamma} \quad & TL(f_c) \\ \text{subject to} \quad & t_{avg,p} = \frac{\sum_{e_p} t_{e_p} A_{e_p}}{\sum_{e_p} A_{e_p}} \leq \frac{t_{min} + t_{max}}{2} \qquad \forall p \end{aligned} \quad (20)$$

where the TL computation has been discussed in Section 4, and the same constraints as (F1) on the maximum material usage have been introduced.

3.3. Solution of the problem

The formulated optimization problems in Equation 19 and Equation 20 are solved through the Method of Moving Asymptotes (MMA) [15], as a gradient-based optimizer searching for local optimality. In order to iteratively update the designs until convergence, the sensitivities of objective function and constraints with respect to changes in the design variables are needed to be computed. We here compute the sensitivities analytically through the adjoint method, where the expression for eigenvalue sensitivities can be found in [1], and the expression of the TL sensitivity can be found in [2].
As the local optimum found by the MMA generally depends on the choice of the initial guess, we perform multiple optimizations for each design case when considering different uniform initial thickness distributions. This mitigates the drawbacks related to the chosen local optimality algorithm and allows to better approximate the global optimum.

Table 1: Material and geometrical properties of the considered single PMMA panels and double glazing panels.

	ρ	E	ν	η	Dim.	t_{min}	t_{max}
Single PMMA	1275 $\frac{kg}{m^3}$	4.5 GPa	0.35	0.06	1 m × 1 m	15 mm	60 mm
Double glazing	2500 $\frac{kg}{m^3}$	62 GPa	0.24	0.01	1.25 m × 1.5 m	pl.1: 3 mm pl.2: 4 mm	pl.1: 5 mm pl.2: 8 mm

Table 2: Final value of the objective functions, obtained for the optimized layouts.

	f_c	Obj. (F1)	Obj. (F2)
Single PMMA	500 Hz	$\beta(^*)$ = 0.3218	TL = 41.37 dB
	1000 Hz	$\beta(^*)$ = 0.2057	TL = 41.46 dB
Double glazing	f_{msm} = 222.86 Hz	$\beta(^*)$ = 0.083	TL = 39.89 dB

(*) $\beta = 0.1225 \Rightarrow$ 1/3-octave band with no eigenfrequencies

$\beta = 0.4142 \Rightarrow$ octave band with no eigenfrequencies

4. OPTIMIZATION RESULTS AND DISCUSSION

4.1. Single panel

As a first case, we consider the design of a single PMMA panel. Table 1 lists the related material properties (mass density ρ, Young modulus E, Poisson ration ν, damping loss factor η), along with the panel dimensions and the range of variation for thickness $[t_{min}, t_{max}]$. The considered 1 m × 1 m panel is dicretized by 50 × 50 finite elements, and the filter radius r_{min} is set to twice the dimension of one single element. We also note that, due to the varying thickness, the designed panel will be translucent but not fully transparent.

The PMMA panel is optimized when considering two different target frequencies f_c = 500 Hz and f_c = 1000 Hz, and the related layouts when considering also the two different formulations of the optimization problem are shown in Figures 2 and 3. It can be seen how more complex layouts, with finer details, are designed at higher frequencies, as a more local modulation of the stiffness and mass properties through thickness is needed to control the response related to higher order modes.

Also, the corresponding final values of the objective functions β and TL are shown in the first row of Table 2. Here we also show the correspondence between the objective function β of formulation (F1) and the width of the obtained frequency band with no eigenfrequencies: for both the considered target frequencies, layouts without eigenfrequencies in a band wider than a 1/3-octave band are obtained.

The TL curves of the optimized layouts are shown in Figures 4 and 5, where a comparison with a uniform plate with constant $\gamma = 0.5$, i.e. constant thickness equal to $(t_{min} + t_{max})/2$, is also shown. We see how, for the same total amount of used material and mass, a non-uniform thickness distribution allows for superior sound insulation properties around the targeted frequency, with TL improvements around 5-10 dB. Similar final performances are obtained when using the two different formulations, as in both cases the algorithm uses the same strategy of suppressing resonance dips. It can be however seen how (slightly) wider frequency bands with no resonance dips around f_c are created when using formulation (F1), and a (slightly) higher TL at f_c is obtained when using formulation (F2).

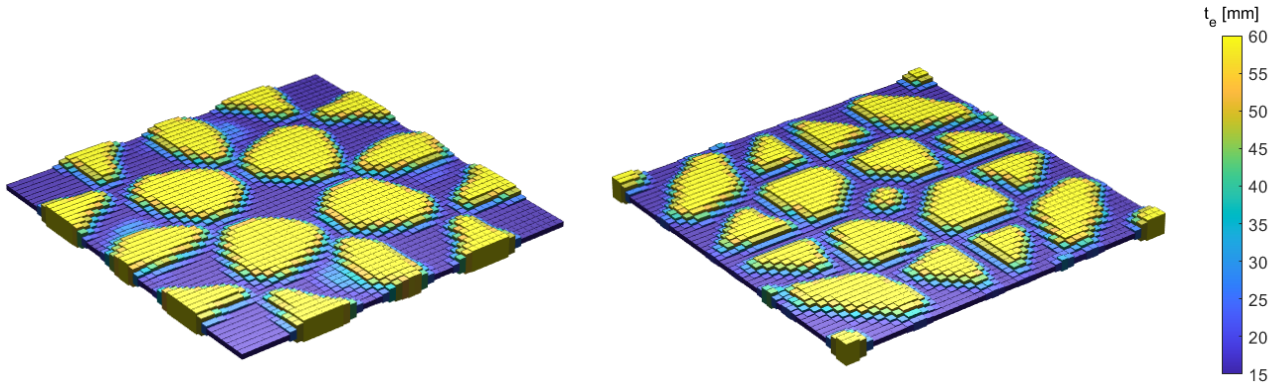

(a) Optimized single PMMA panel layout for f_c = 500 Hz, using formulation (F1).

(b) Optimized single PMMA panel layout for f_c = 500 Hz, using formulation (F2).

Figure 2: Optimized single PMMA panel layouts for f_c = 500 Hz.

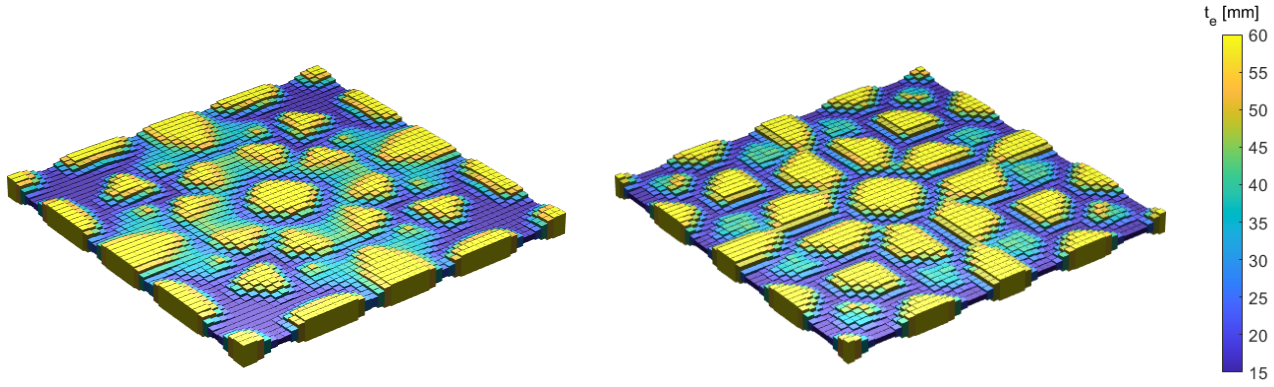

(a) Optimized single PMMA panel layout for f_c = 1000 Hz, using formulation (F1).

(b) Optimized single PMMA panel layout for f_c = 1000 Hz, using formulation (F2).

Figure 3: Optimized single PMMA panel layouts for f_c = 1000 Hz.

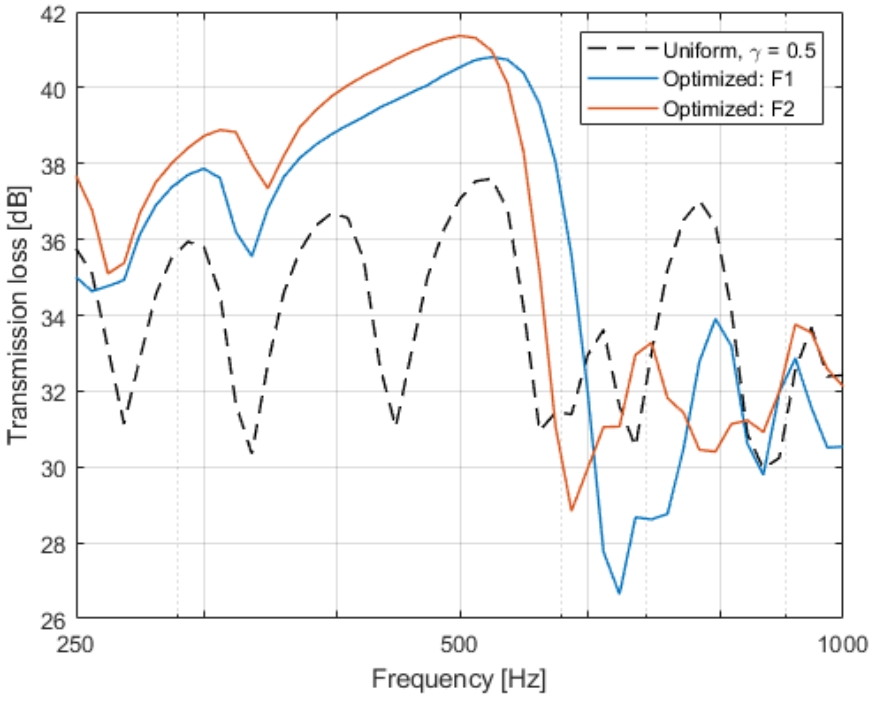

Figure 4: Transmission loss of the single PMMA panel layouts optimized for f_c = 500 Hz.

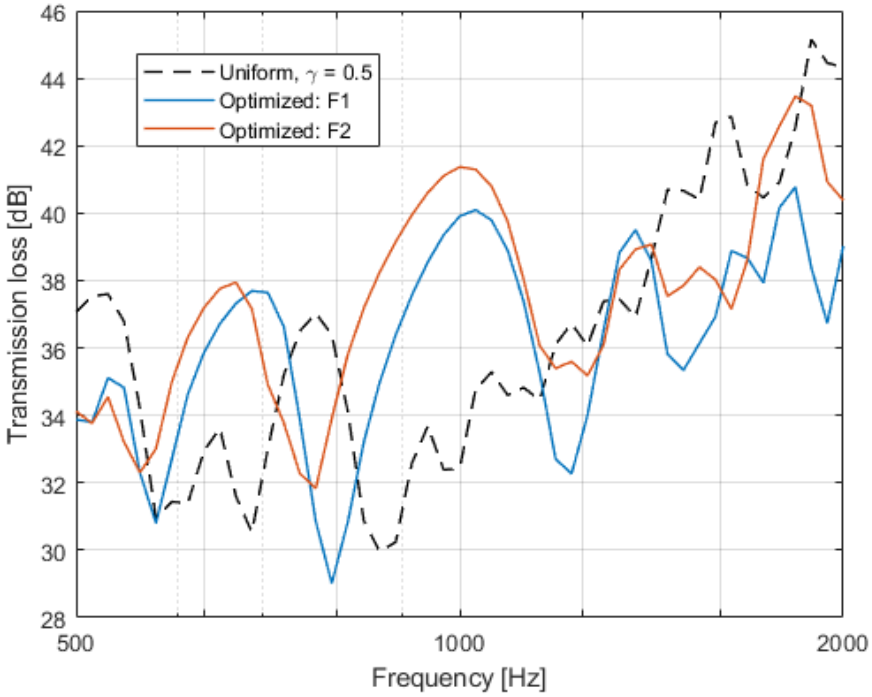

Figure 5: Transmission loss of the single PMMA panel layouts optimized for $f_c = 1000$ Hz.

4.2. Double panel

The second considered case is related to the design of a translucent double glazing with non uniform material distribution. The material properties, panel dimensions and thickness ranges are again shown in Table 1. The 1.25 m × 1.5 m panel is here discretized by 50 × 60 finite elements, with a filter radius r_{min} again set to twice the dimension of one element.

In this case, the considered baseline uniform panel is constituted by uniform plates with 4 mm and 6 mm thickness, separated by a 12 mm cavity, denoted as a 4-12-6 glazing. The target frequency for the optimization f_c will be equal to the mass-spring-mass resonance f_{msm} of the double glazing: this frequency is characterized by a sourrounding band with low TL, with both plates that vibrate almost as rigid masses and the air cavity that is compressed as a spring. For uniform panels, the mass-spring-mass resonance frequency can be approximated as [16]:

$$f_{msm} = \frac{c_a}{2\pi}\sqrt{\frac{\rho_a}{L_z}\left(\frac{1}{\rho t_1}+\frac{1}{\rho t_2}\right)} \tag{21}$$

Figure 6 shows the sound transmission loss of a uniform 4-12-6 glazing, and highlights the frequency band with reduced TL close to $f_{msm} = 222.86$ Hz. The objective of the design is therefore to obtain a non-uniform double glazing panel with superior vibroacoustic behavior, when keeping the same plate masses as the uniform 4-12-6 glazing panel.

The optimized double glazing layouts when using the two formulations (F1) and (F2) are shown in Figure 7, and the corresponding final values of the objective functions are shown in the second row of Table 2. The related TL curves compared with the uniform 4-12-6 glazing are instead shown in Figure 8. In the case of the double glazing, we can see how maximizing the width of the frequency band with no eigenfrequencies (formulation (F1)) successfully suppresses resonance dips around $f_c = f_{msm}$, but it is not enough to achieve an adequate increase of the TL. A direct maximization of TL (formulation (F2)) allows to achieve a clear peak in the TL, and the related layout overperforms the uniform 4-12-6 panel by ∼15 dB at the target frequency.

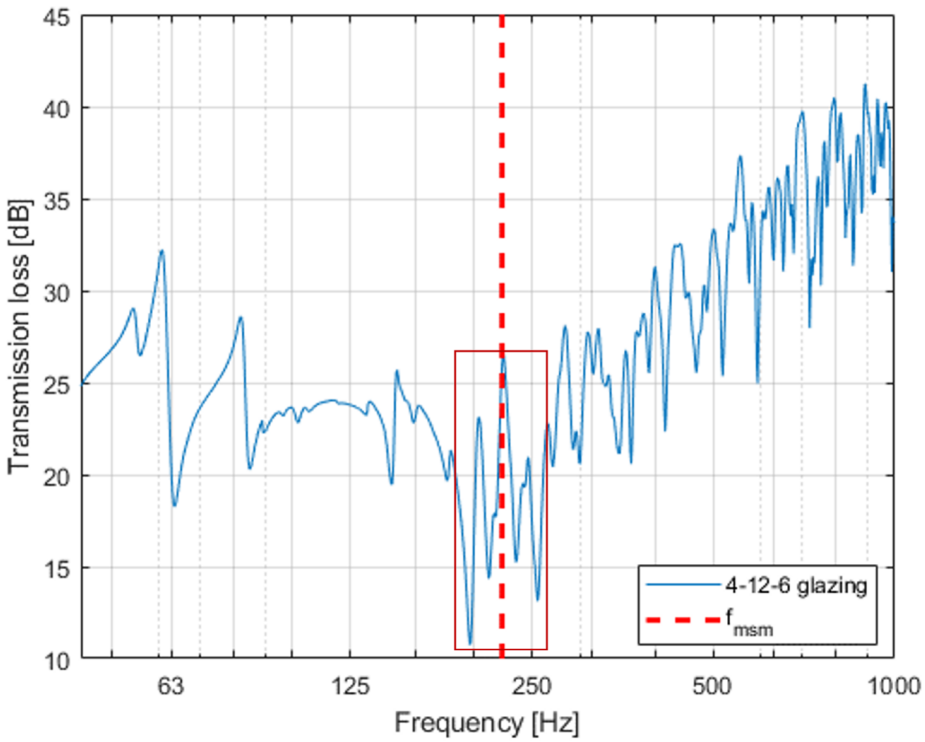

Figure 6: Sound transmission loss (TL) of a uniform 4-12-6 double glazing, with highlighted mass-spring-mass resonance frequency f_{msm} and related frequency band with low TL.

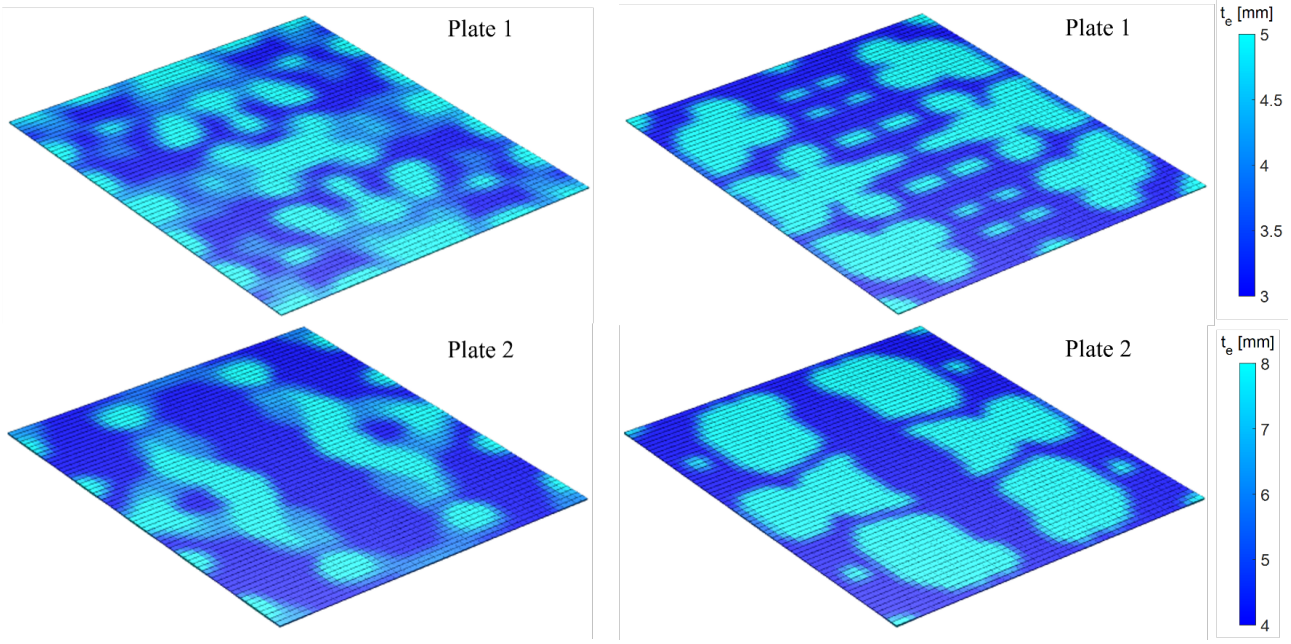

(a) Optimized double glazing layout using formulation (F1).

(b) Optimized double glazing layout using formulation (F2).

Figure 7: Optimized double glazing layouts.

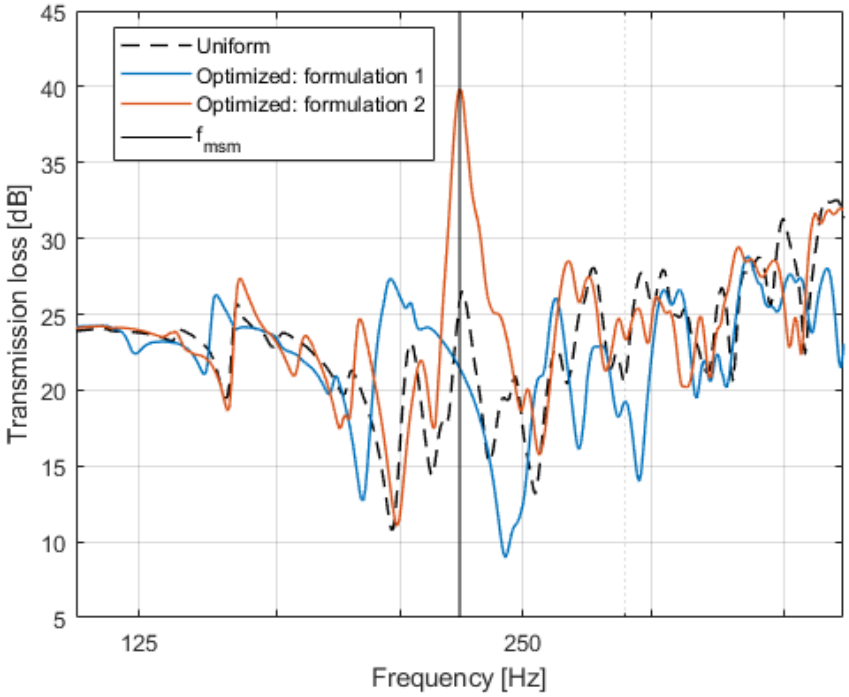

Figure 8: Transmission loss of the optimized double glazing panel layouts.

5. CONCLUSIONS

In this paper, topology optimization has been used to increase the vibroacoustic properties of single and double panels around a specific target frequency, through a non uniform distribution of the plate thicknesses. When constraining the maximum material usage, two design objectives have been proposed, i.e. suppressing the resonance transmission loss dips by pushing the system eigenfrequencies away from a target frequency, and directly maximizing the value of the transmission loss at the target frequency. In a first design case, related to single PMMA panels, the layouts optimized with the two formulations have shown a similar improvement of the transmission loss performance, overperforming corresponding uniform panels with equal mass by 5-10 dB around the target frequency. In a second design case, related to double glazing panels, the results have shown how simply suppressing the resonance dips is not enough to adequately improve the sound insulation properties, but a direct maximization of the sound transmission loss is needed. In this last case it has been possible to overperform the transmission loss of a uniform panel with same mass by $\approx$15 dB at the target frequency.

The proposed approach can be extended to target a wider band improvement of the vibroacoustic behaviour in panels, e.g. by maximizing a single-number rating for airborne sound insulation [17].

ACKNOWLEDGEMENTS

The presented research has been carried out within the framework of the ERC Starting Grant 714591 VirBAcous. The authors gratefully acknowledge the financial support of the European Research Council (ERC).

REFERENCES

[1] M.P. Bendsøe and O. Sigmund. *Topology optimization: theory, methods and applications*. Springer, Berlin, second edition, 2004.

[2] Jan Van den Wyngaert, Mattias Schevenels, and Edwin Reynders. Acoustic topology optimization of the material distribution on a simply supported plate. pages 1208–1215. Ochmann, Vorlander and Fels, 2019.

[3] Edwin Reynders, Robin S. Langley, Arne Dijckmans, and Gerrit Vermeir. A hybrid finite element – statistical energy analysis approach to robust sound transmission modeling. *Journal of Sound and Vibration*, 333(19):4621–4636, 2014.

[4] Daniele Giannini, Francesco Braghin, and Niels Aage. Topology optimization of 2d in-plane single mass mems gyroscopes. *Structural and Multidisciplinary Optimization*, 62, 10 2020.

[5] Daniele Giannini, Niels Aage, and Francesco Braghin. Topology optimization of mems resonators with target eigenfrequencies and modes. *European Journal of Mechanics - A/Solids*, 91:104352, 07 2021.

[6] Quhao Li, Qiangbo Wu, Ji Liu, Jingjie He, and Shutian Liu. Topology optimization of vibrating structures with frequency band constraints. *Structural and Multidisciplinary Optimization*, 63:1–16, 03 2021.

[7] Daniele Giannini, Mattias Schevenels, and Edwin Reynders. Topology optimization of plate structures for sound transmission loss improvement in specific frequency bands. In *Proceedings of the 12th European Congress and Exposition on Noise Control Engineering, Euronoise 2021*, pages 1435–1442, Madeira, Portugal, 2021.

[8] Jan C.E. Van den Wyngaert, Mattias Schevenels, and Edwin P.B. Reynders. Predicting the sound insulation of finite double-leaf walls with a flexible frame. *Applied Acoustics*, 141:93–105, 2018.

[9] P.J. Shorter and R.S. Langley. Vibro-acoustic analysis of complex systems. journal of sound and vibration. *Journal of Sound and Vibration*, 288:669–699, 12 2005.

[10] P. J. Shorter and R. S. Langley. On the reciprocity relationship between direct field radiation and diffuse reverberant loading. *The Journal of the Acoustical Society of America*, 117(1):85–95, 2005.

[11] Carolina Decraene, Arne Dijckmans, and Edwin Reynders. Fast mean and variance computation of the diffuse sound transmission through finite-sized thick and layered wall and floor systems. *Journal of Sound and Vibration*, 422:131–145, 05 2018.

[12] Edwin Reynders, Cedric Van hoorickx, and Arne Dijckmans. Sound transmission through finite rib-stiffened and orthotropic plates. *Acta Acustica united with Acustica*, 102:999–1010, 11 2016.

[13] R. S. Langley. Numerical evaluation of the acoustic radiation from planar structures with general baffle conditions using wavelets. *The Journal of the Acoustical Society of America*, 121(2):766–777, 2007.

[14] Fengwen Wang, Boyan Lazarov, and Ole Sigmund. On projection methods, convergence and robust formulations in topology optimization. *Structural and Multidisciplinary Optimization*, 43:767–784, 06 2011.

[15] Krister Svanberg. The method of moving asymptotes—a new method for structural optimization. *International Journal for Numerical Methods in Engineering*, 24(2):359–373, 1987.

[16] J.H. Rindel. *Sound insulation in buildings*. CRC Press, Boca Raton, FL, 2018.

[17] International Organization for Standardization. *ISO 717-1: Acoustics – Rating of sound insulation in buildings and of building elements – Part 1: Airborne sound insulation*, 2020.